J Mater Sci (2008) 43:1324–1333
DOI 10.1007/s10853-007-2229-y

Oxidation of NdFeB-type magnets modified with additions of Co, Dy, Zr and V

I. Skulj · H. E. Evans · I. R. Harris

Received: 7 February 2007 / Accepted: 15 October 2007 / Published online: 12 December 2007

Abstract The oxidation characteristics of NdFeB alloys, modified by additions of Co up to 10 at.% and with minor additions of Dy, Zr and V, have been examined in this article over the temperature range 250–500 °C. The surface oxide consisted of an outer surface layer of polycrystalline haematite, regardless of Co content, and an inner layer of Co-modified magnetite. Underlying this two-layer surface oxide was an extensive internal oxidation zone (IOZ) formed as a result of preferential reaction with oxygen of the magnetic phase, $Nd_2(Fe, Co)_{14}B$. The IOZ consisted of a bcc solid solution of Fe and Co and contained a fine dispersion of Nd-rich oxide particles. The zone grew by inward oxygen diffusion, principally along high-angle grain boundaries within the Fe-rich matrix. The thickening of the IOZ occurred with parabolic kinetics but at a rate which decreased with increasing alloy Co content by a consistent factor of 2–3 in parabolic rate constant at all test temperatures. The activation energy for the growth of the IOZ lay in the approximate range 91–104 kJ/mol for the various alloys but there did not appear to be a systematic variation with alloy composition.

Introduction

NdFeB-type magnets have good magnetic properties but their oxidation performance at elevated temperatures remains a problem [1–4]. The oxidation reaction results in the formation of two external scales, of Fe_2O_3 and Fe_3O_4, and an internally oxidised zone (IOZ), which is, typically, an order of magnitude thicker than the surface oxide layers and represents the main form of degradation resulting from the oxidation reaction. The main oxidising reaction in the formation of this zone is the dissociation of the $Nd_2Fe_{14}B$ phase to form oxides of neodymium and, probably, boron in a matrix of unoxidised iron [2–4]. This matrix phase of the IOZ is α-Fe and consists of columnar grains of approximately 200 nm width oriented approximately at right-angles to the specimen surface, i.e. in the direction of inward oxygen transport [2]. These grain boundaries, which are high-angle, are thought to provide short-circuit diffusion paths for the inward transport of oxidation. Amorphous precipitates, probably of NdO, approximately 2 nm in diameter, exist within the α-Fe grains [2].

The oxidation behaviour of NdFeB alloys has previously been determined by following different test parameters such as oxygen pressure [5], thermo-magnetic measurements [6], thermo-gravimetric measurements [7] or IOZ thickness [2, 3, 8]. The last, in particular, confirmed that the IOZ thickness, χ, increased parabolically with time, t, i.e.

$$\chi = (k(T)t)^{1/2} \quad (1)$$

where $k(T)$ is the parabolic rate constant which, itself, is a function of temperature. The value of $k(T)$ will also depend on microstructural features, high-angle grain boundaries in particular, within the IOZ since inward oxygen diffusion occurs by such short-circuit diffusion paths. It can then be anticipated that changes to the basic $Nd_{16}Fe_{76}B_8$ composition might also change the microstructure of the IOZ and have a corresponding effect on the oxidation kinetics. Indeed, previous work on the effect of additions such as Co, Dy, Zr and V to NdFeB materials [6] suggests that an

I. Skulj · H. E. Evans (✉) · I. R. Harris
Department of Metallurgy and Materials, School of Engineering, University of Birmingham, Birmingham B15 2TT, UK
e-mail: h.e.evans@bham.ac.uk

Present Address:
I. Skulj
Institute of Metals and Technology, 1000 Ljubljana, Slovenia

improvement in oxidation resistance can result. The purpose of the work described in this article was to undertake a systematic study of the influence of Co, in particular, on oxidation kinetics but also to examine the role of minor alloying additions. In this article, the growth kinetics of the IOZ will be presented for the modified alloys at various temperatures and the nature of the oxidation attack will be described.

Experimental

The magnetic alloys (Table 1) used for this research were prepared via the hydrogen-decrepitation powder-metallurgy/roller-milled route. The base alloy $Nd_{16}Fe_{76}B_8$ was crushed into smaller pieces (2–5 mm), decrepitated in 1 bar of H_2 at 50 °C and then roller-milled for 20 h in cyclohexane. This powder ($\sim$5 μm diameter) was then blended with an appropriate amount of NdH_2, Co, DyH_2, Zr or V powders. The mixed powders were tumbled for 1 h in an air-tight 250 cm^3 vessel containing ball bearings, then sealed in a rubber tube and aligned in a magnetic field of 4.5 T. The aligned powder mixture was isostatically pressed at 1,400 kg/cm^2 into a green compact and sintered in an evacuated furnace at 1,070 °C for 1 h. To improve the magnetic properties the materials were annealed in vacuum at 630 °C for 1 h, followed by rapid cooling.

Disc specimens, of 10 mm diameter and 4 mm height, were oxidised in static laboratory air in an open furnace at 250–500 °C for periods of 24–144 h. The products formed as a result of the oxidation reaction were identified by X-ray diffraction (XRD) using Cu K_α radiation in a Siemens D500 diffractometer. Oxidised samples were also cross-sectioned and polished for SEM to investigate the microstructure of the oxidised layers formed on the surface. Cross-sections were also prepared for TEM investigations using FIB sectioning.

Results and discussion

Oxidation kinetics

The typical morphology of the oxidation product is shown in Fig. 1 for the ternary NdFeB alloy but is characteristic of all the alloys tested. The IOZ is clearly evident in this figure due to the contrast difference when using the SEM in back-scattered mode. The thickness of the IOZ is much greater than the surface oxide which, as shown by Li et al. [2] for this ternary alloy, consists of an outer layer of Fe_2O_3 and an inner layer of Fe_3O_4. Fuller characterisation of the oxides formed in the more complex alloys tested here will be presented later. The emphasis in this section will be on the kinetics of growth of the IOZ.

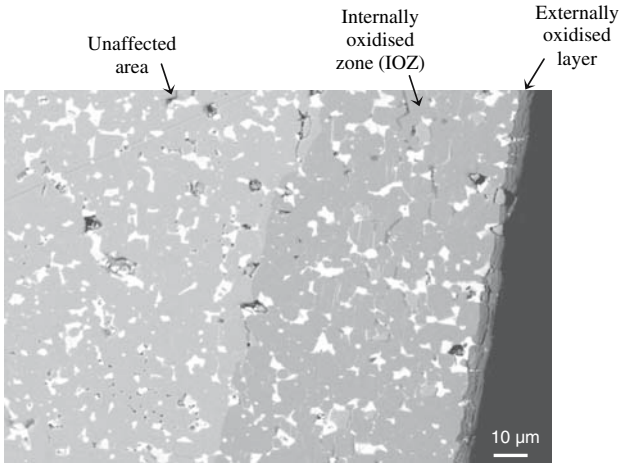

Fig. 1 Cross-section of the oxidised layers of the NdFeB alloy (M1) oxidised at 400 °C for 96 h

The increasing thickness of the IOZ with oxidation exposure is shown in Fig. 2 for various alloy compositions at 400 °C and in Fig. 3 for alloy M5 ($Nd_{16}(Fe_{67}Co_{10})B_7$) at various temperatures. In each case, the kinetics are reasonably parabolic and can be expressed by Eq. 1. The best-fit lines have here been extrapolated back to zero time and show that there is no incubation period prior to the start of internal oxidation. This suggests that the surface oxides, which form in these alloys (Fig. 1), fail to offer protection even in the early stages of oxidation when they would be expected to be less cracked and more adherent. This observation agrees with the view of Li et al. [2], based on the unmodified NdFeB alloy.

The effect of additions to the base alloy of composition $Nd_{16}Fe_{76}B_8$ (Table 1) can be seen clearly in Fig. 2 and

Table 1 Initial compositions of the alloys used in this work, at.%

Alloy	Nd	Fe	B	Co	Dy	Zr	V
M1	16.0 ± 1.0	76.0 ± 1.0	8.0 ± 0.5	–	–	–	–
M2	16.0 ± 1.0	73.3 ± 1.0	7.7 ± 0.5	3.0 ± 0.5	–	–	–
M3	16.0 ± 1.0	71.5 ± 1.0	7.5 ± 0.5	5.0 ± 0.5	–	–	–
M4	16.0 ± 1.0	69.6 ± 1.0	7.4 ± 0.5	7.0 ± 0.5	–	–	–
M5	16.0 ± 1.0	66.9 ± 1.0	7.1 ± 0.5	10.0 ± 0.5	–	–	–
M6	14.0 ± 1.0	66.4 ± 1.0	6.9 ± 0.5	9.7 ± 0.5	3.0 ± 0.5	–	–
M7	13.9 ± 1.0	66.2 ± 1.0	6.9 ± 0.5	9.7 ± 0.5	3.0 ± 0.5	0.3 ± 0.1	–
M8	13.9 ± 1.0	66.2 ± 1.0	6.9 ± 0.5	9.7 ± 0.5	3.0 ± 0.5	–	0.3 ± 0.1

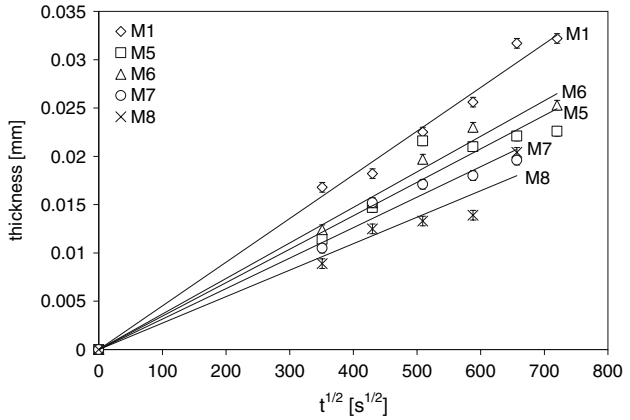

Fig. 2 Comparison of the IOZ thicknesses at 400 °C for the different alloys

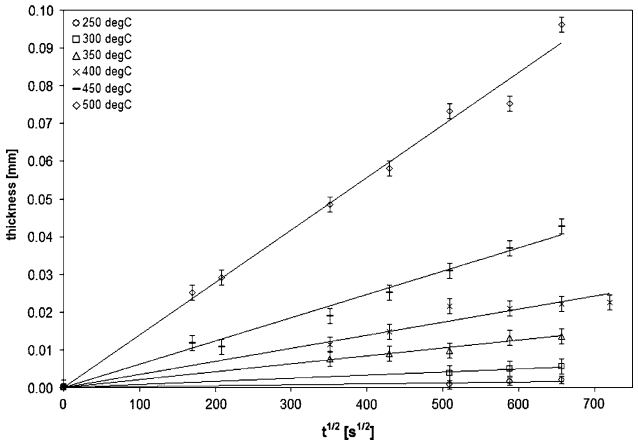

Fig. 3 Thicknesses of the IOZ for samples of the M5 alloy oxidised at temperatures between 250 and 500 °C. The lines drawn represent parabolic kinetics and extrapolate to zero exposure time. The error bars represent the upper and lower bounds of approximately four measurements

Table 2 and show a tendency for a decreasing oxidation rate with increasing Co content. The addition of Dy to the alloy with a 10 at.% Co content (M6) results in a similar reduction of IOZ growth rate compared with that of M1 while V (M8) or Zr (M7) in addition to 10 at.% Co and

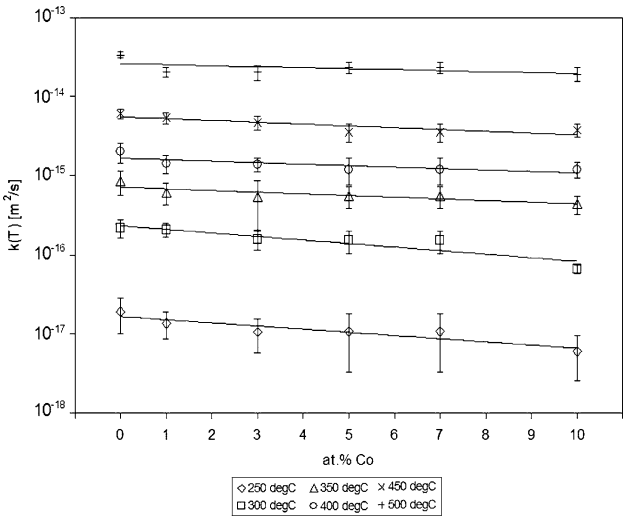

Fig. 4 The dependence on alloy Co content of the rate constant, $k(T)$, for growth of the IOZ at different oxidation temperatures

3 at.% Dy further improves the situation. These trends were present at all test temperatures as can be appreciated from Table 2 which gives the parabolic rate constants for thickening of the IOZ, as calculated from Eq. 1, for all alloys. Co additions, up to 10 at.%, produce a reduction in rate constant of typically a factor 2–3 at each of the test temperatures used, as can be seen in Fig. 4. This corresponds roughly to 1/3 less penetration depth in the high-Co alloy than in the simple $Nd_{16}Fe_{76}B_8$ alloy at any given time and temperature.

Exposures to these test temperatures impair the magnetic properties of all the alloys even in the absence of oxidation [9] but the loss of the magnetic phase ($Nd_2(Fe,Co)_{14}B$) in the IOZ during oxidation exacerbates matters. For the simple Co-bearing alloys, for example, the loss of coercivity after oxidation in air at 400 °C for 96 h can be as high as 30% but this loss is much smaller in Dy-containing alloys, e.g. M6.

The temperature dependence of the parabolic rate constant for IOZ growth for the 10 at.% Co alloy (M5) is shown in the Arrhenius plot of Fig. 5, i.e. fitted to the equation:

Table 2 Experimentally determined oxidation rate constants, $k(T)$, (m^2/s)

Alloy	250 °C	300 °C	350 °C	400 °C	450 °C	500 °C
M1	1.93×10^{-17}	2.22×10^{-16}	8.55×10^{-16}	2.04×10^{-15}	6.13×10^{-15}	3.39×10^{-14}
M2	1.37×10^{-17}	2.09×10^{-16}	6.15×10^{-16}	1.44×10^{-15}	5.44×10^{-15}	2.08×10^{-14}
M3	1.06×10^{-17}	1.56×10^{-16}	5.40×10^{-16}	1.40×10^{-15}	4.73×10^{-15}	2.06×10^{-14}
M4	1.08×10^{-17}	1.53×10^{-16}	5.62×10^{-16}	1.21×10^{-15}	3.57×10^{-15}	2.34×10^{-14}
M5	0.61×10^{-17}	0.67×10^{-16}	4.42×10^{-16}	1.20×10^{-15}	3.79×10^{-15}	1.94×10^{-14}
M6	0.65×10^{-17}	1.33×10^{-16}	4.74×10^{-16}	1.38×10^{-15}	3.76×10^{-15}	1.62×10^{-14}
M7	0.56×10^{-17}	0.85×10^{-16}	4.60×10^{-16}	1.04×10^{-15}	3.20×10^{-15}	1.23×10^{-14}
M8	0.43×10^{-17}	0.89×10^{-16}	3.21×10^{-16}	0.74×10^{-15}	1.57×10^{-15}	0.90×10^{-14}

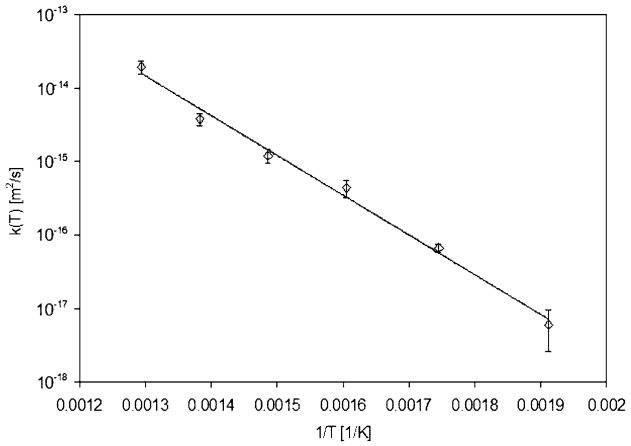

Fig. 5 Arrhenius plot for the M5 alloy. The error bars represent the standard deviation for each temperature

$$k(T) = k_0 \exp\left(-\frac{E_a}{8.314\,T}\right) \quad (2)$$

where the activation energy, E_a, and pre-exponential term, k_0, were found to be 103,600 J/mol and 15.7 × 10^{-8} m^2 s^{-1}, respectively. These and the corresponding values for the other alloys are given in Table 3 together with estimated standard deviations. A comparison of these mean values using the *t*-test shows that the differences between the majority of them are not significant (e.g. M5 and M6; M4 and M6; M4 and M2) but can be so at the extremes. In general, though, there seems little basis for assuming that there are systematic variations of the activation energy with alloy content.

This point can also be appreciated from a comparison of earlier measurements of the activation energy for the base $Nd_{16}Fe_{76}B_8$ alloy with those obtained in the present study. Thus, Li et al. [2] obtained a value of ~112 kJ/mol after combining their results with those of Edgley et al. [4]. This compares with the current value of 93.1 kJ/mol for this particular alloy. These two values of activation energy for the same alloy show a similar spread in values to that shown in Table 3 for all the alloys tested here. These

Table 3 Values of activation energy and pre-exponential factors for all alloys

Alloy	Composition	E_a (kJ/mol)	$k_0 \times 10^8$ (m^2/s)
M1	$Nd_{16}Fe_{76}B_8$	93.1 ± 5	4.7 ± 0.2
M2	$Nd_{16}Co_3Fe_{73.3}B_{7.7}$	91.4 ± 3	2.6 ± 0.3
M3	$Nd_{16}Co_5Fe_{71.5}B_{7.5}$	95.0 ± 4	4.4 ± 0.6
M4	$Nd_{16}Co_7Fe_{69.6}B_{7.4}$	94.0 ± 6	3.5 ± 1.2
M5	$Nd_{16}Co_{10}Fe_{66.9}B_{7.1}$	103.6 ± 4	15.7 ± 3.0
M6	$Nd_{14}Dy_3Co_{9.7}Fe_{66.4}B_{6.9}$	97.8 ± 5	6.0 ± 1.5
M7	$Nd_{13.9}Dy_3Co_{9.7}Fe_{66.2}B_{6.9}Zr_{0.3}$	97.8 ± 2	4.9 ± 0.9
M8	$Nd_{13.9}Dy_3Co_{9.7}Fe_{66.1}B_{6.9}V_{0.3}$	92.9 ± 2	1.4 ± 0.5

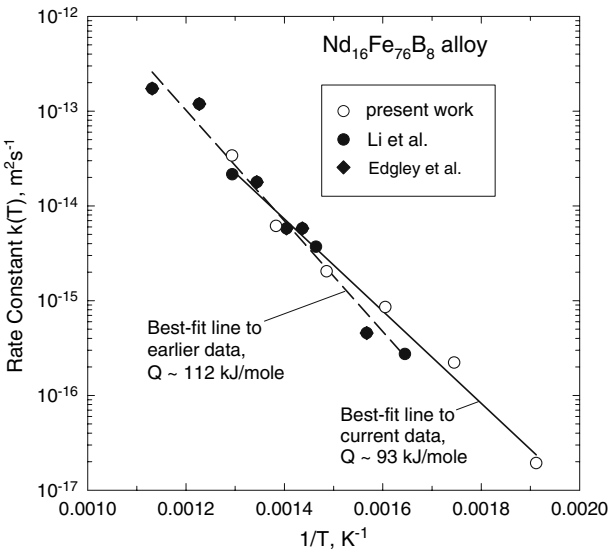

Fig. 6 An Arrhenius plot comparing the present results on the M1 NdFeB alloy with the earlier data of Edgley et al. [4] and of Li et al. [2]

earlier data on NdFeB are compared with the present results in Fig. 6 and, in fact, show that there is good *numerical* agreement of the values of rate constants for all three data sets at moderate to high temperatures, even though there appears to be a large difference in activation energy.

It was argued by Li et al. [2] that the thickening of the IOZ in their $Nd_{16}Fe_{76}B_8$ alloy was controlled by the diffusion of oxygen along high-angle grain boundaries within the oxidised zone. This was inferred because anticipated *lattice* diffusion rates, extrapolated from higher-temperature diffusion data, would result in penetration depths orders of magnitude smaller than those observed. The similarity in the values of activation energy and penetration rates, found here over the range of alloys, with those reported by Li et al. indicate that a similar process is occurring. It will be shown later, however, that the matrix grain size of the IOZ in the present 10 at.% Co alloy is much more variable than that reported by Li et al. for the ternary $Nd_{16}Fe_{76}B_8$ material.

The rate of inward diffusion of oxygen in these alloys is very much higher than any outward diffusion of Nd from the unreacted alloy to the internal reaction front to form Nd-rich oxide particles. Under these circumstances, the generalised theory of internal oxidation developed by Wagner [10] may be simplified by assuming that the solute (Nd) is effectively immobile. The parabolic rate constant, $k(T)$, for the thickening of the IOZ is then obtained as:

$$k(T) = \frac{\chi^2}{t} = \frac{2N_O^{(Fe,Co)}D_O}{\nu N_{Nd}} = \frac{2P_O}{\nu N_{Nd}} \quad (3)$$

Table 4 Oxygen permeability in the IOZ at 400 °C

Alloy	Composition	$(N_O^{(Fe,Co)} D_O) \times 10^{17}$ (m^2 s^{-1})
M1	$Nd_{16}Fe_{76}B_8$	12.04 ± 0.73
M2	$Nd_{16}Co_3Fe_{73.3}B_{7.7}$	8.50 ± 1.08
M3	$Nd_{16}Co_5Fe_{71.5}B_{7.5}$	8.26 ± 0.78
M4	$Nd_{16}Co_7Fe_{69.6}B_{7.4}$	7.14 ± 0.80
M5	$Nd_{16}Co_{10}Fe_{66.9}B_{7.1}$	7.08 ± 0.78
M6	$Nd_{14}Dy_3Co_{9.7}Fe_{66.4}B_{6.9}$	8.14 ± 0.54
M7	$Nd_{13.9}Dy_3Co_{9.7}Fe_{66.2}B_{6.9}Zr_{0.3}$	6.14 ± 0.56
M8	$Nd_{13.9}Dy_3Co_{9.7}Fe_{66.1}B_{6.9}V_{0.3}$	4.37 ± 0.52

where χ is the thickness of the IOZ, t is the exposure time, $N_O^{(Fe,Co)}$ and N_{Nd} are the atomic fraction of oxygen in the (Fe, Co) matrix of the IOZ and the atomic fraction of neodymium in the unreacted alloy, respectively. D_O is the effective diffusion coefficient of oxygen within the (Fe, Co) matrix of the IOZ, P_O is the oxygen permeability within the zone and v is the stoichiometric ratio in the oxide precipitates formed within the IOZ. Here, $v = 1$ for the NdO particles thought [2] to be present within the IOZ for the ternary $Nd_{16}Fe_{76}B_8$ alloy and, for the present calculations, assumed to exist also in the present modified alloys. Using the values of the rate constant $k(T)$ given in Table 2, taking $v = 1$ and $N_{Nd} = 0.118$, for the case of oxidation of the $Nd_2Fe_{14}B$ phase, values of oxygen permeability can be calculated from Eq. 3. These values for an oxidation temperature of 400 °C are collected in Table 4 for each of the alloys and plotted against Co content in Fig. 7. It can be seen that there is a marked reduction in oxygen permeability of approximately 40% over this composition range. From Eq. 3, it can be appreciated that this decrease could arise from a combination of reduced oxygen solution within the alloy with increasing Co content (the parameter $N_O^{(Fe,Co)}$ in Eq. 3) or to a reduction in the effective oxygen diffusion coefficient D_O. This latter would arise if the average grain size within the IOZ were to increase with Co additions.

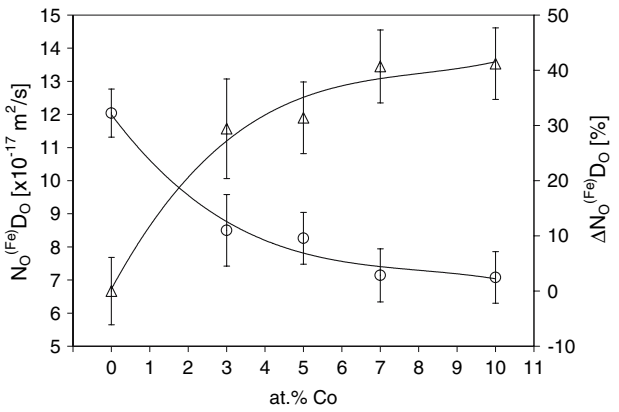

Fig. 7 The decrease of oxygen permeability in numeric (circle) and percentage terms (triangle) in the IOZ at 400 °C as a function of Co addition to the NdFeB alloy. The error bars reflect the standard deviation of the thickness measurements

Nature of the oxidation products

EDX analysis of the outer surface oxide layer, shown for the ternary alloy in Fig. 1, indicated that it was Fe-rich for all the alloys tested and this was confirmed by XRD analysis of the oxidised bulk samples as shown in Fig. 8 for a selection of the alloys tested. Little information could be obtained from buried layers in these specimens but it is clear that α-Fe_2O_3 was a dominant product in the surface oxide layer. This agrees with previous XRD and TEM analyses [2, 4] and with Mössbauer spectroscopy [4, 11].

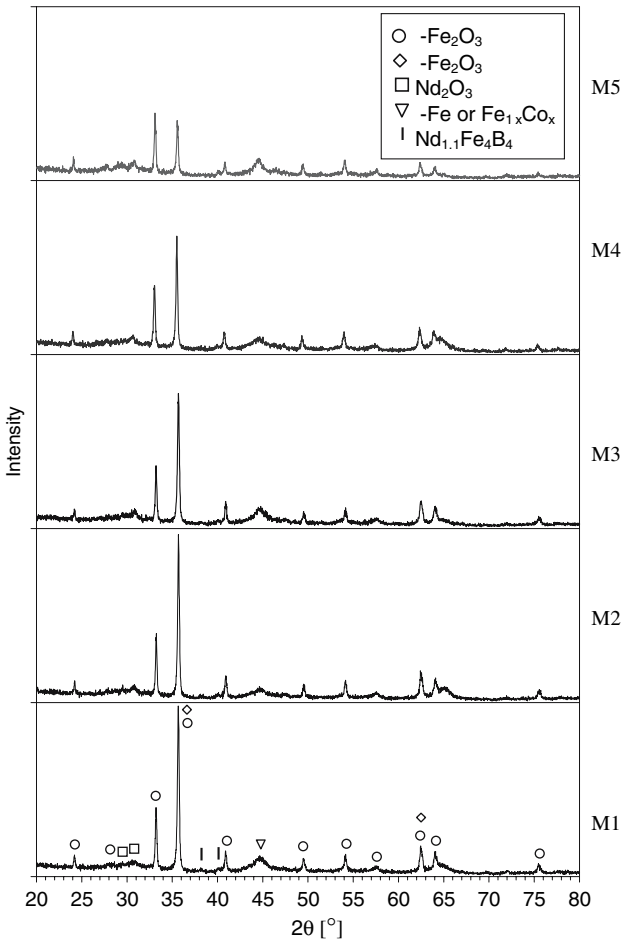

Fig. 8 Representative XRD spectra from bulk specimens having a range of Co additions from 0 (M1) to 10 at.% (M5) after oxidation at 400 °C for 96 h. Detailed compositions of each alloy are given in Table 1

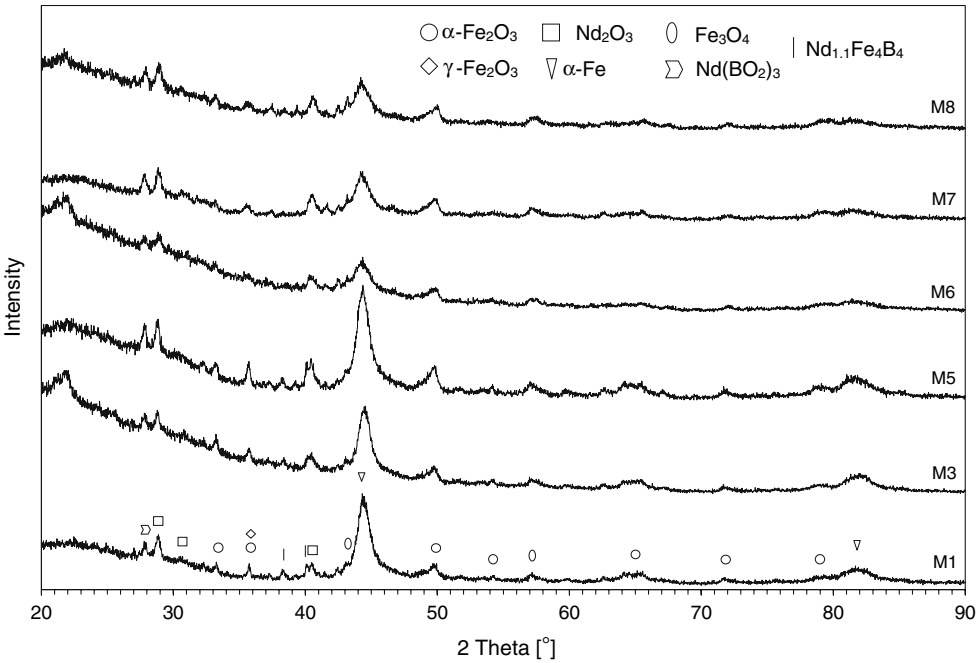

Fig. 9 XRD spectra obtained from the spalled powder of various alloys after oxidation at 400 °C for 96 h showing the influence of Co and other additions to the base Nd–Fe–B composition (M1). Alloy compositions are given in Table 1. The arrowed peak for alloy M6 may be Dy_2O_3

A more useful XRD characterisation of the layers underlying the outer haematite layer was obtained by exposing the oxidised specimens to laboratory air at room temperature for a period of some days. It was then found that the IOZ spalled along its interface with the unaffected alloy substrate due, presumably, to corrosion in humid air. The spalled product was often in the form of powder and it was this that was examined by XRD. Typical XRD spectra from such material showing the influence of various alloy additions are given in Fig. 9. These results confirm the presence of α-Fe_2O_3 but it is now clear that magnetite (Fe_3O_4) is also present in the Co-free alloy (M1) and, as a modified version containing Co, ($(Fe, Co)_3O_4$), in the Co-bearing alloys. It will be shown below that this magnetite exists as a discrete layer underlying the outer haematite layer. The dominant peak in these spectra corresponds to the α-Fe phase of the IOZ in the M1 alloy and to $Fe_{1-x}Co_x$ in the Co-bearing alloys. This identification has again been confirmed by Mössbauer spectroscopy [11] on the present alloys. In contrast, the magnetic phase, $Nd_2(Fe, Co)_{14}B$, is absent from all the spectra of the oxidised layers for all the alloys, indicating that this has dissociated during the oxidation reaction. This again agrees with previous observations on ternary NdFeB alloys [e.g. 2]. These spectra also indicate that boron has been oxidised and exists in a complex oxide with neodymium.

The duplex structure of the surface oxide can be seen in more detail in the cross-sectional TEM image of Fig. 10 of a sample of the M5 alloy oxidised for 72 h at 350 °C. The surface oxide can be seen clearly to consist of an outer 300 nm thick layer consisting of grains approximately 50 nm in diameter overlying an inner featureless layer some 50–100 nm thick. Selected area electron diffraction patterns confirm this outer layer to be Fe_2O_3 and the inner layer to be magnetite, in agreement with the XRD results.

Structure of the IOZ

It can be appreciated from the TEM micrograph of Fig. 10 that the IOZ has a microstructure which suggests directionality of grains in the growth direction, i.e. normal to the specimen surface. This columnar morphology is similar to that found previously in the base NdFeB alloy by Li et al. [2]. A more extensive cross-sectional image for alloy M5 (10 at.% Co) after oxidation at 350 °C for 72 h is shown in Fig. 11.

It can be seen from Fig. 11 that, although the matrix grains within the IOZ have a columnar morphology, their width varies with location within the zone. At the original $Nd_2Fe_{14}B$ grain boundaries, shown dotted in this figure, the grains are narrow, typically 50 nm wide, but are substantially larger (~600 nm) at locations positioned within the former $Nd_2Fe_{14}B$ grains. Diffraction patterns, taken from different grains within the IOZ, are also included in Fig. 11. These show that all the grains sampled are of Fe–Co type with a bcc structure but have different orientations. As previously reported [11], Co is present as a solid solution in α-Fe.

The differences in grain width between original grain boundary and grain interior locations (Fig. 11) suggest that new small α-(Fe, Co) grains are nucleated when the front of

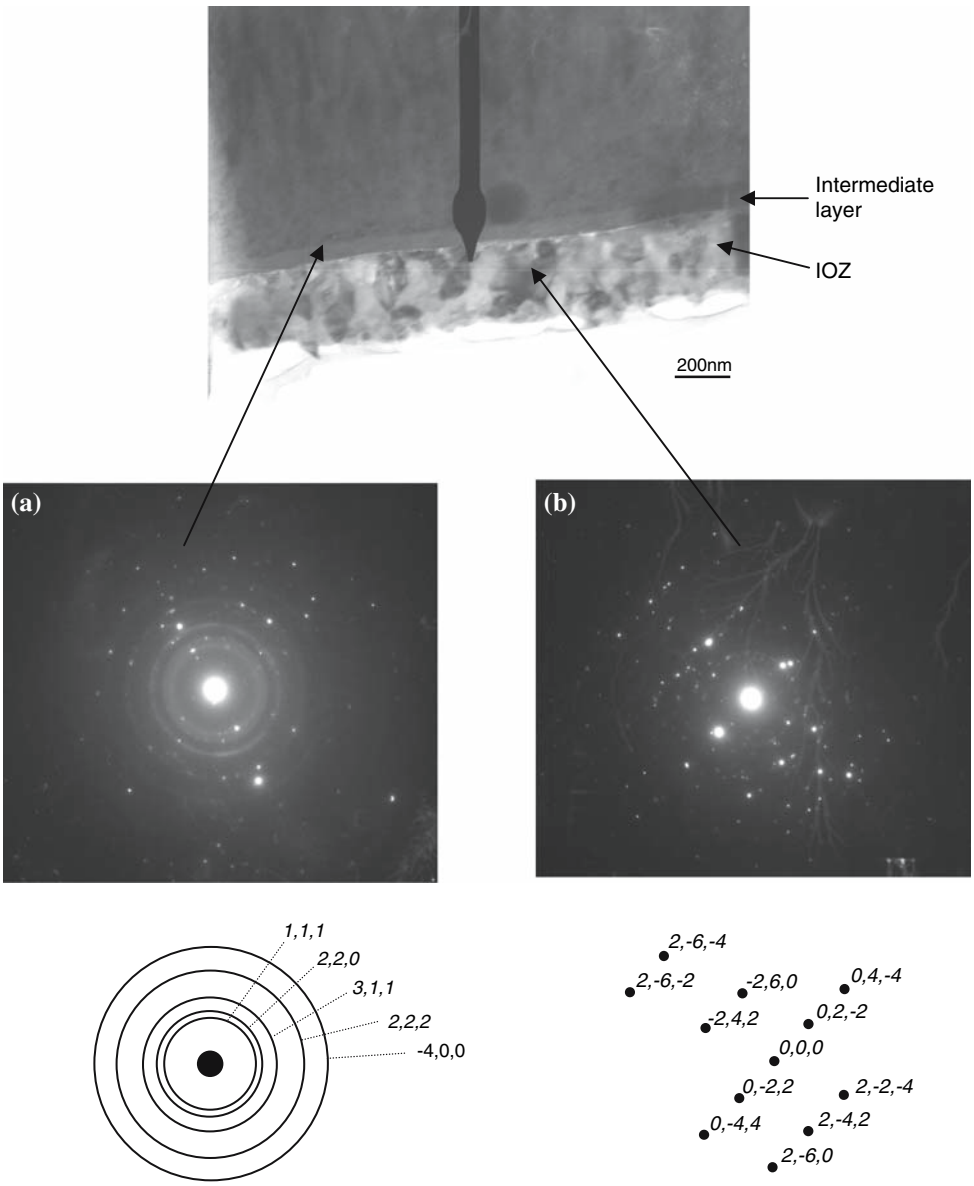

Fig. 10 Cross-sectional TEM image of a sample of alloy M5 oxidised for 72 h at 350 °C showing the outer oxide layers. The diffraction patterns show the outermost layer to be haematite and the underlying layer to be magnetite

the IOZ reaches an original $Nd_2Fe_{14}B$ grain boundary. This probably is a consequence of the change in orientation between the original grains. Subsequent inward growth of the α-(Fe, Co) grains into the alloy as the IOZ thickens leads, however, to an increase in grain width. This is not due to conventional grain growth, resulting from accumulated time at temperature, since fine grains continue to exist within the IOZ at locations nearer to the specimen surface, i.e. structures formed early in the oxidation process. This resistance to conventional grain coarsening is not unexpected since the dispersion of Nd-oxide particles within the IOZ will inhibit grain boundary migration.

It is suggested that the increase in width of the α-(Fe, Co) grains, described earlier, is a consequence of the dynamic oxidation process in that some of the first-formed small grains cannot extend as quickly as others forming the IOZ. The process is shown schematically in Fig. 12. In this figure, the original $Nd_2Fe_{14}B$ grain boundaries are considered to be delineated by a Nd-rich phase and are shown speckled. They become consumed as the IOZ grows into the alloy, as illustrated in the middle and lower diagrams. In the early stages of this process (top diagram), numerous α-(Fe, Co) grains will have formed but only a fraction of these will be bounded by high-angle grain boundaries. This is a crucial factor in the growth of these grains since it is along such fast-diffusion paths that oxygen penetrates into the IOZ [2]. Those grains bounded by low-angle boundaries will not grow or grow much more slowly and will

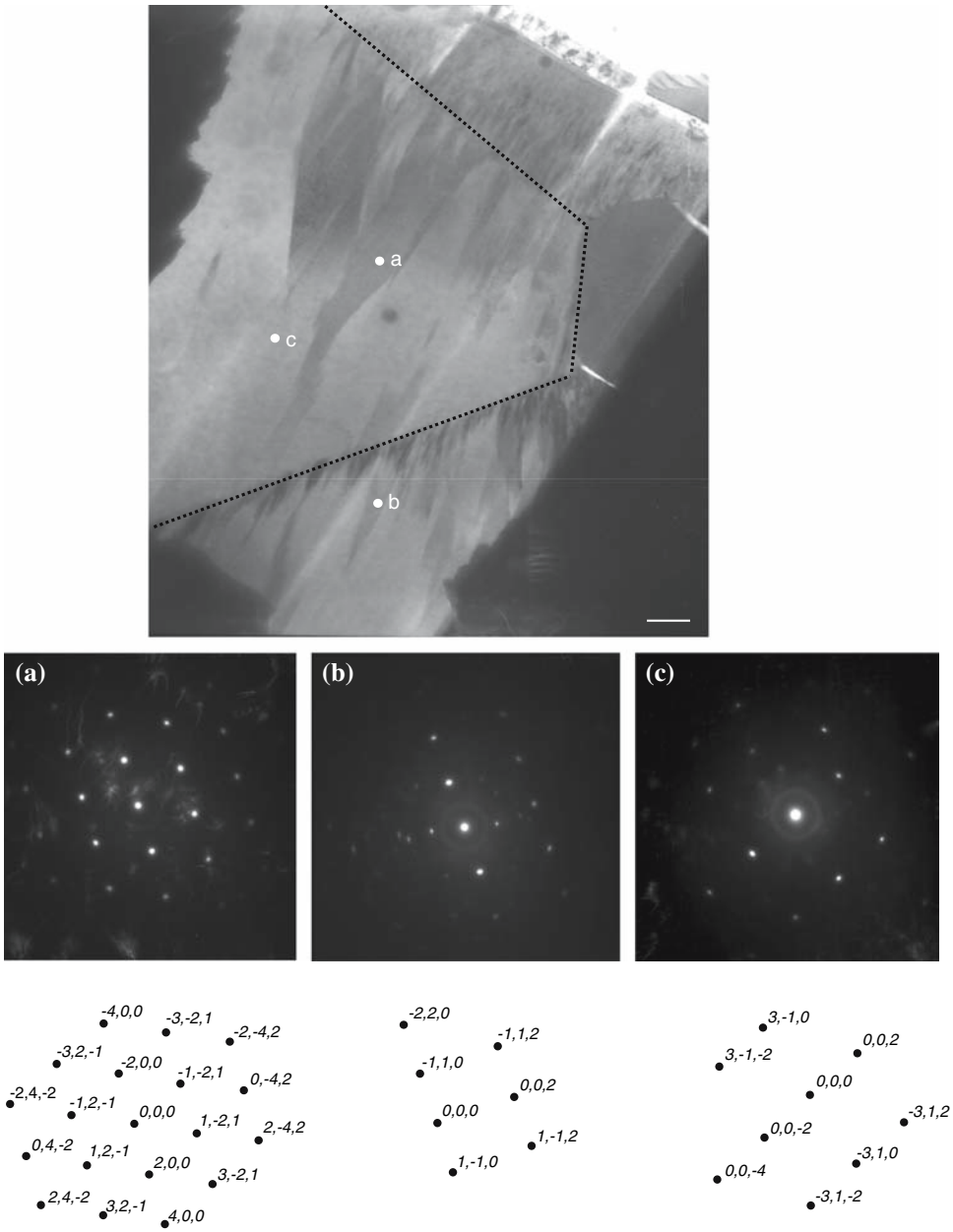

Fig. 11 Cross-sectional TEM and SAD patterns for alloy M5 after oxidation for 72 h at 350 °C

tend to be confined to those regions of the IOZ in which they originally nucleated. This overall process is shown schematically in Fig. 12.

This incoming oxygen flux partitions at the interface of the IOZ with the unoxidised alloy. Some reacts with $Nd_2Fe_{14}B$ in the immediate vicinity of the high-angle grain boundary to increase the thickness of the IOZ locally but the remainder diffuses laterally along the IOZ interface (the lateral arrows in Fig. 12). This latter flux also reacts with the underlying $Nd_2Fe_{14}B$ grain to form a wedge at the interface but the shape of this wedge is determined by the relative magnitudes of the interfacial diffusion rate and reaction rate of the oxygen flux. One extreme example, shown schematically in Fig. 13, arises when the reaction rate is very much higher than the lateral diffusion rate along the IOZ interface. In this case, the IOZ grows in the form of narrow protuberances into the underlying alloy and a highly non-planar interface ensues. In the other extreme, lateral diffusion rates are high and near-uniform conversion of the original matrix occurs along the IOZ interface. In this case, the IOZ interface would be planar. This appears to be the approximate situation in the present alloys as can be appreciated from Fig. 1. It is possible, in principle, for the *reaction* rate to control the rate of formation of the IOZ.

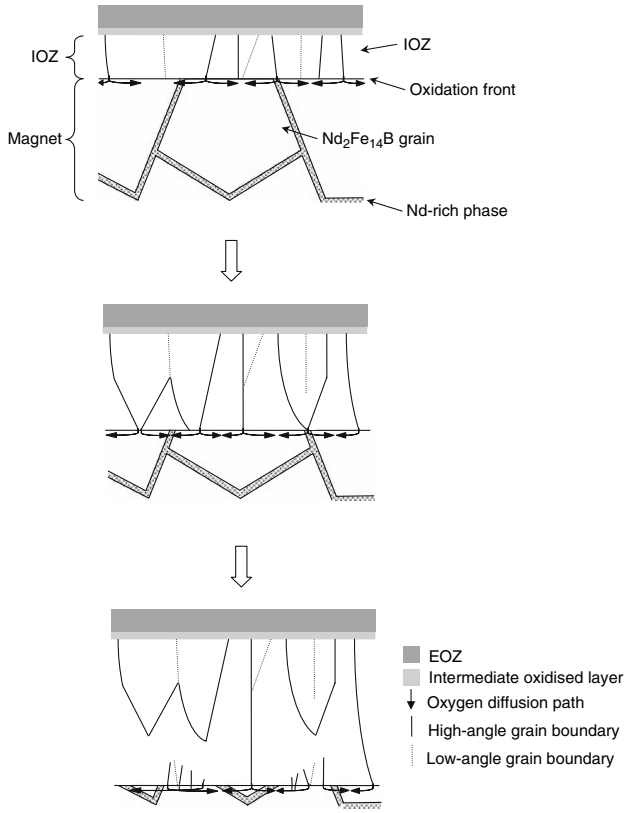

Fig. 12 Schematic diagram showing the process of grain coarsening as the IOZ thickens with time by inward oxygen diffusion along α-(Fe, Co) high-angle grain boundaries. The figure is not to scale

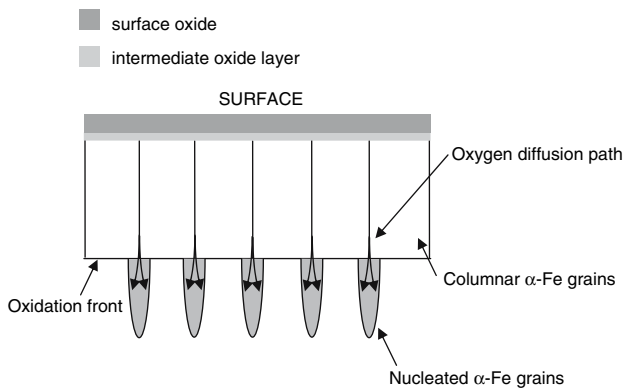

Fig. 13 The expected morphology of the interface between the IOZ and the matrix alloy if lateral diffusion rates of the incoming oxygen flux were very much less than the reaction rates

However, since the kinetics of growth of the latter are parabolic, it is more reasonable to think that the supply of oxygen to the interface through the IOZ controls its growth rate.

It has been shown earlier in this article that the kinetics of thickening of the IOZ were parabolic and could be described by Eq. 3. This implies that the value of the diffusion coefficient, D_O, for oxygen diffusion within the IOZ must be invariant with time. As implied above, this diffusion coefficient incorporates contributions from lattice transport but mainly from grain boundary transport. The value of D_O will, thus, depend on the lateral spacing of the high-angle grain boundaries within the IOZ. Parabolic kinetics for the thickening of the IOZ will then occur only if the average value of the number density of high-angle grain boundaries, along a plane parallel to the alloy surface is independent of distance from the surface.

Conclusions

NdFeB alloys, modified by additions of Co up to 10 at.% and with minor additions of Dy, Zr and V, have been oxidised in air over the temperature range 250–500 °C. Although friable Fe-rich oxides (haematite and Co-modified magnetite) form on the alloy surface, they appear to have no influence on the principal degradation process of the growth of an internally oxidised zone (IOZ). The thickening of this zone occurs with parabolic kinetics but at a rate, which decreases with increasing alloy Co content by a consistent factor of 2–3 in rate constant over the alloy range at all test temperatures. The activation energy for the growth of the IOZ lay in the approximate range 91–104 kJ/mol for the various alloys but there did not appear to be a systematic variation with alloy composition. The reaction kinetics were interpreted in terms of Wagner's theory of internal oxidation in which the solute, Nd in this case, could be considered immobile by comparison with the diffusion of oxygen. The measured activation energies then relate to the permeability of oxygen within the IOZ but the controlling process is likely to be transport of oxygen along matrix grain boundaries within this zone.

The IOZ is formed as a result of preferential reaction of the magnetic phase, $Nd_2(Fe, Co)_{14}B$, with oxygen. The matrix phase of the IOZ is a bcc solid solution of Fe and Co and has a columnar grain structure which tends to coarsen as the oxidation front traverses an original alloy grain. This coarsening has been associated with the loss of relatively low-angle grain boundaries which carry less of the inward oxygen flux. Regeneration of fine (Fe, Co) grains occurs as the oxidation front encounters an original alloy grain boundary and the above cycle of grain coarsening re-starts.

Acknowledgements The authors are grateful to the Engineering and Physical Sciences Research Council (grant GR/N64755/01) and Marie Curie Fellowships for their financial support for this work. Thanks are also given to Less Common Metals Ltd. for the provision of the material used in this study.

References

1. Blanc R, Adler E (1987) Proceedings of the 9th International workshop on rare earth magnets and their applications. Bad Soden, Germany, p 537
2. Li Y, Evans HE, Harris IR, Jones IP (2002) Oxid Met 59:167
3. Edgley DS, Le Breton J-M, Lemarchand D, Harris IR, Teillet J (1993) J Magn Magn Mater 128:L1
4. Edgley DS, Le Breton J-M, Steyaert S, Ahmed FM, Harris IR, Teillet J (1997) J Magn Magn Mater 173:29
5. Higgins BE, Oesterreicher H (1987) IEEE Trans Magn 23:92
6. Lemarchand D, Delamare J, Vigier P (1992) J Appl Phys 72:1996
7. Osawa Z, Higuchi M, Hinohara S (1992) J Mater Sci 27:5445
8. Steyaert S, Le Braton J-M, Teillet J (1996) J Phys Condens Matter 8:10721
9. Skulj I (2005) PhD thesis. The oxidation behaviour of Co and Dy modified NdFeB magnets. The University of Birmingham, Birmingham, UK
10. Wagner C (1959) Z Elektrochem 63:772
11. Skulj I, Douvalis AP, Harris IR (2005) J Alloys Compd 407:304